Hybrid Optoelectronic Backplane Bus for Multiprocessor-Based Computing Systems

Chunhe Zhao, Jian Liu and Ray T. Chen
Microelectronics Research Center
Department of Electrical and Computer Engineering
The University of Texas at Austin
Austin, TX 78712

Yung S. Liu
GE Corporate Research and Development Center
Schenectady, NY12301

Abstract

The architecture of a hybrid electrical and optical backplane with multiple bus lines for high performance bus is proposed and bus systems with 2-bus lines at a wavelength of 850 nm are experimentally demonstrated, with a size of collimation lens (here we used graded index (GRIN) lenses) and level of collimation-limited separation of 1.5 mm between the two bus lines. For the new bus system containing multiple bus lines and 9 processor/memory boards, VCSELs (Vertical Cavity Surface Emitting Lasers) and photodetector arrays, such parameters as power budget, misalignment and packaging related issues are discussed. With the introduction of GRIN lenses into the backplane system, it is found that not only can the signal beam from the VCSELs get collimated, but the angular tolerance of the system is greatly enhanced. The optical backplane bus system developed here is transparent to higher level bus protocols, thus can support standard backplane buses such as Futurebus+, Multi-bus II, and VMEbus.

1. Introduction

Over the past decade, the demand for more computing power has increased to such an extent that no single processor can provide the solutions in many applications. As a result, various efforts were made to build multiprocessor systems. The system based on electrical backplane buses, whose basic structure is shown in Fig. 1, has been prevailing in the commercial market mainly due to the simplification of design and low cost. However, as the signal speed increases along the backplane, the transmission line effects become dominant[1,2]. Even in the most advanced electronic backplane interconnection prototypes, such as IBM's backplane, the bottleneck occurs at 150 Mbit/s. Although advanced buses like Futurebus+[3] guarantee an incident wave switching, other inherent problems still degrade the performance significantly[4]. As faster processors arise, the electrical backplane buses can no longer supply the bandwidth required for high performance multiprocessor systems.

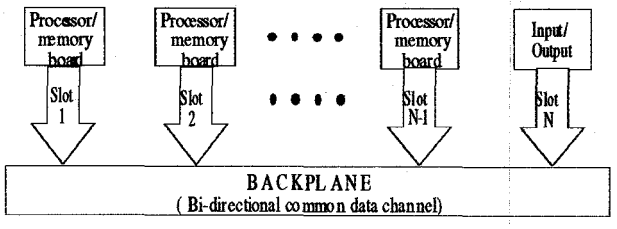

Fig. 1. Diagram of bus-based multiprocessor systems.

In an effort to increase the interconnection capacity, optics has been considered as an alternative for a long time[4]. Nonetheless, the burden of electrical-to-optical and optical-to-electrical conversions has prevented optics from growing as a viable solution. Recent development of efficient optoelectronic devices, especially in forms of arrays, has stimulated the research seeking for feasible optical solutions. In spite of these efforts, no general optical backplane compatible with existing electrical buses has been announced.

In order to provide a competitive optical solution, we have developed a bi-directional optical backplane[5]. Unlike other optical backplanes aimed at special purpose computers[6], the backplane we reported is for general purpose; thus, is compatible with standard multiprocessor backplane buses such as Futurebus+, Multi-bus II, etc. In this paper we further proposed a hybrid electrical/optical backplane. It incorporates multiple bus lines instead of a single bus line as previously reported, hence increases performance and the degree of integration of the backplane system. The application of the basic design method as in our previous developed backplane system ensures the compatibility of the new backplane bus system with standard multiprocessor backplane buses. But the multi-bus line characteristic greatly enhences the bandwidth of

0-8186-7591-8/96 $5.00 © 1996 IEEE
Proceedings of MPPOI '96

the bus system. Because of its planar optical interconnect structure and bi-directional signal transmission characteristic, the new architecture is simple for transceiver design and easy for system packaging.

2. Implementation of bi-directional optical backplane bus

The basic elements employed in our bi-directional optical backplane bus structure are arrays of doubly exposed holograms in conjunction with a glass substrate. The coupling diagrams for a doubly exposed hologram are shown in Fig. 2. Fig. 2 (a) demonstrates the configuration when optical signal is incident onto the hologram vertically, which is the case when where the output signal from the VCSEL is coupled into the backplane bus. Fig. 2(b) simulates the case where the optical signal input hits the multiplexed hologram inside the glass substrate. For both cases, the optical signals are diffracted by the multiplexed holograms under Bragg condition. The cross-coupling effect[7] of the multiplexed holograms divides the incident signals $\vec{k}$ into upward output $\vec{k}'_{up}$, downward output $\vec{k}'_{down}$, and substrate guided modes $\vec{k}'$, $\vec{k}'_1$ and $\vec{k}'_2$, which keep on propagating inside the glass substrate via total internal reflection (TIR).

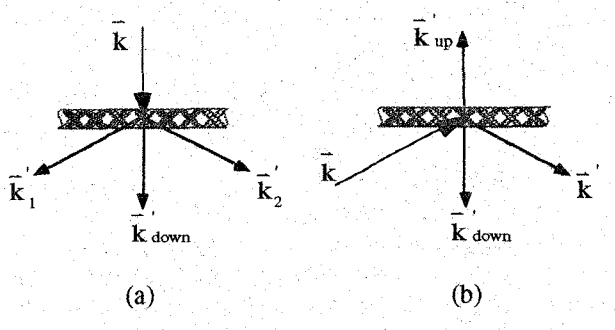

Fig. 2. Coupling diagram of optical signals by doubly exposed hologram gratings.

Employment of a single array of doubly exposed holograms on a glass substrate leads to the bi-directional optical backplane bus system as shown in Fig. 3, as having been proposed in Ref. 5. The thickness of the substrate and the bouncing times of optical signal inside the substrate can be adjusted to meet the standard 3 cm separation between neighboring boards. Furthermore, as shown in Fig. 3, to reduce the power consumption, a layer of high reflection coating is coated on the back surface of the backplane.

Based on the above scheme, a bi-directional optical backplane with a single bus line has been demonstrated with nine channels at a signal of data transfer rate 1.2 Gbit/sec operating at a wavelength of 1.3 μm[5]. Theoretical results aimed at minimize the output fluctuations among different channels are also reported, thus, the overall performance is optimized.

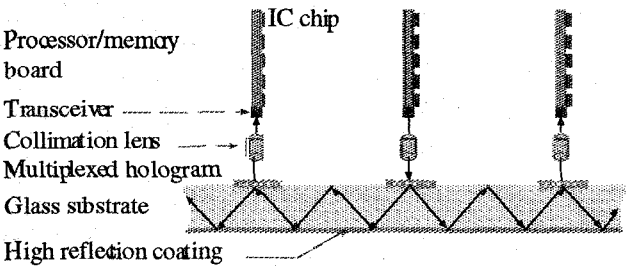

Fig. 3. Realization of bi-directional optical backplane bus using doubly exposed holographic gratings in conjunction with a glass substrate.

3. Hybrid backplane bus with multiple bus lines

The optical bi-directional backplane demonstrated previously[5] has only one bus line. Furthermore, as one can see, for the architecture shown in Fig. 3, signal transmitting and receiving should have the same input/output window, which would introduce drawbacks in the wiring of the signal and packaging of the system. A hybrid electrical/optical backplane scheme can easily overcome these difficulties by expanding the above backplane into one with multiple bus lines utilizing the $\vec{k}'_{down}$ beam as in Fig. 2, and incorporating arrays of transmitter and receiver multichip modules(MCM's) on each side of the waveguiding channel as indicated in Fig. 4. We utilize the fanouts directed to the opposite side of the transmitters. This arrangement will result in a simpler transceiver design and ease the system packaging. Although we use the same waveguiding structure provided by the array of multiplexed holograms and the waveguiding plate, the overall design must be changed from Fig. 3 to be integrated with electrical processor/memory boards. The center of one hologram is separated from those of the adjacent ones by 3 cm, which is the standard inter-board distance in electrical backplane environment.

Fig. 5 on next page shows the detailed diagram of waveguiding structure for an array of beams and also indicates the necessary components integrated into the transmitter and receiver multichip modules. As there is another set of fanouts directed to the transmitter modules, the optical isolators are included at the transmitter modules to block them. When the guided optical signals

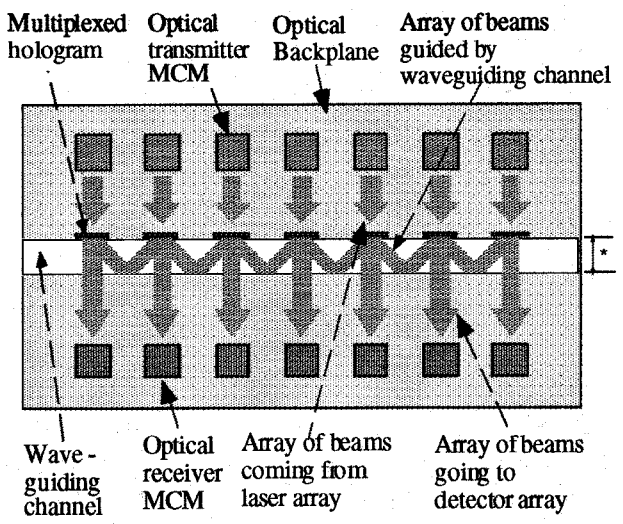

* Width of the waveguiding channel = board separation/2

Fig. 4. Waveguiding structure for multi-channel data path.

are packed closely with each other, crosstalk between the channels may degrade the performance of the system. This mechanisms contributing to this crosstalk can be due to the misalignment of the adjacent channels, or the spreading of the optical signal spots with propagation distance, all of which finally at the output channel leads to the partially overlap among the optical signals from adjacent channels. A detailed effects of inter-channel crosstalk has to be analyzed.

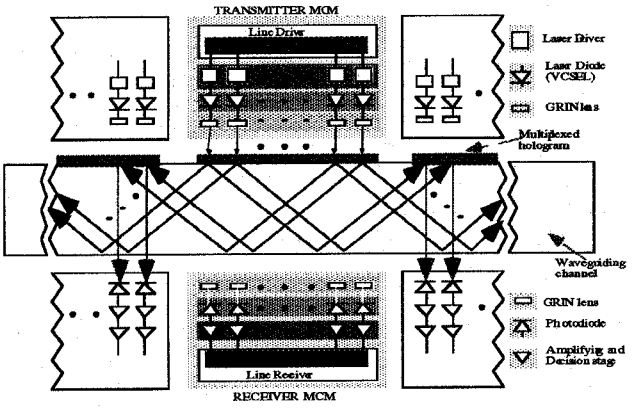

Fig. 5. Detailed diagram of waveguiding structure and transmitter and receiver modules.

4. Experiment results

Fig. 6 shows the fanout configurations of the hybrid backplane bus with 2 bus lines operating at 850 nm which is the most popular wavelength for VCSELs. As for the backplane with a single bus line[5], a cascaded feature is also observed in the case of multiple bus lines.

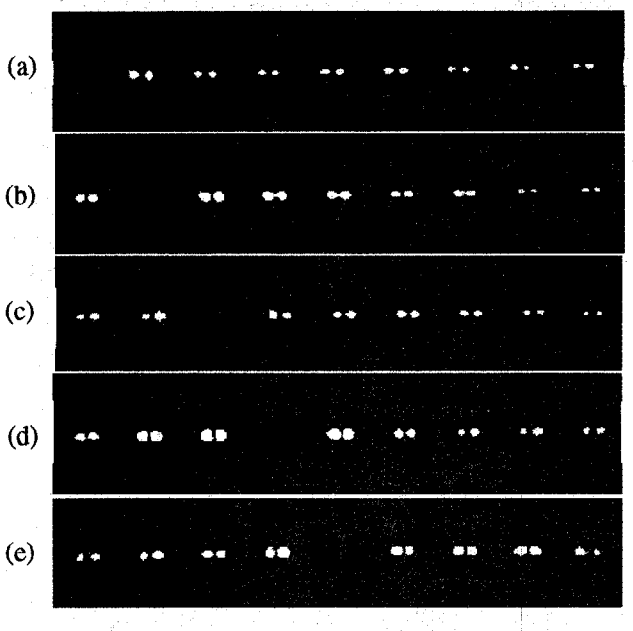

Fig. 6. Photographs with (a) the first, (b) the second, (c) the third, (d) the fourth (e) the fifth channel sending optical signals to the other channels through the bi-directional optical backplane.

The experiment setup is shown in Fig. 7. To simulate VCSEL output, a Ti:Sapphire tunable laser is used to produce the 850 nm signal beam, which is then split into two beams and coupled into two fibers with 1/2-pitch GRIN lenses to simulate the input signal to the backplane. In Fig. 6, the separation of the two neighboring spots between the two bus lines is 1.5 mm, and the limit of this separation will depend on the size of the GRIN lenses and the level of collimation of the two signal beams.

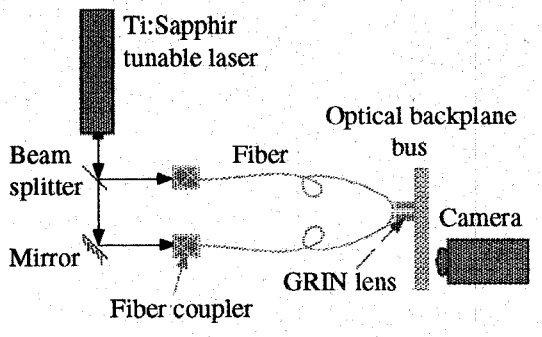

Fig. 7. Experiment setup for the hybrid optical backplane with 2 bus lines.

One different approach to the above backplane with multi-bus line scheme is to arrange all the bus lines parallel to each other, so that the direction of the VCSEL

and detector arrays are parallel to the direction of the processor/memory boards. This case is necessary when the thickness of the boards are limited by the requirements of design and packaging. The output configuration of this approach is shown in Fig. 8. As in Fig. 6, the separation of the two neighboring spots between the two bus lines is also 1.5 mm.

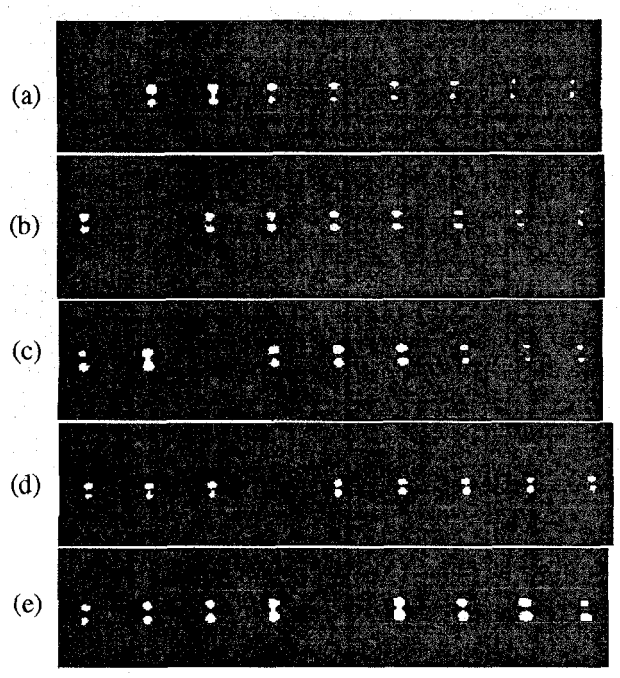

Fig. 8. As Fig. 6, with the direction of the VCSEL and detector arrays are parallel to the direction of the processor/memory boards.

There have been several different approaches[8, 9] to utilize array devices in parallel data links. However, a number of recent attempts were stimulated by the advances of VCSELs, which have evolved into efficient and reliable devices. A VCSEL has many advantageous features for optical interconnection[10]. Small device size, low threshold current, small divergence angle, single longitudinal mode, and circular symmetric emission pattern are some of the most important ones. Another attractive feature of VCSEL technology is the capability of being fabricated into uniform, individually addressable, one and two dimensional arrays[11, 12]. Many optical interconnection systems taking advantage of these VCSEL arrays have been developed or being manufactured[10, 11, 13]. Design issues using VCSEL arrays in free-space optical interconnects were addressed in the previous publication[14].

Fig. 9 shows the picture of the VCSEL we currently used in our lab for the characterization of the hybrid backplane bus. The device has a total of 32-channel array operating at a wavelength of 0.85 μm[15]. The array has 140 μm pitch and typically has an output power about 1-2 mW at 10 mA operating current. As we will see from our following analyses, to collimate the laser beam from the VCSEL, GRIN lenses are introduced into our system. Currently, the commercially available GRIN lenses have minimum radii of 1 mm. So, the minimum channel separation of the hybrid backplane bus system should be 1 mm, which corresponds to at least a separation of 8 channels on the VCSEL array. We expect to present the VCSEL-array-based system in the conference.

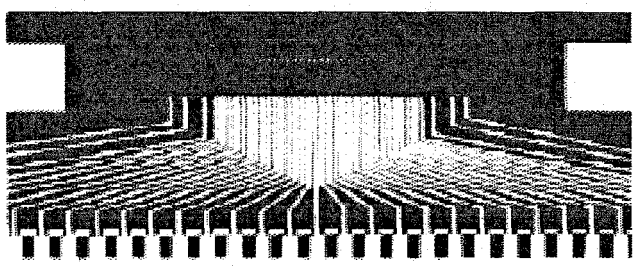

Fig. 9. 32-channel VCSEL array

5. System performance considerations

5.1 Power budget considerations

Power budget is a major concern for both the system design and the device implementation. One of the major results from our previous theoretical calculation[5], aimed at minimizing fluctuations among all the output channels for the demonstrated case, is that the difference between the maximum and the minimum output intensity for different channels is about 17 dB. For each bus line of the hybrid optical backplane bus, the performance can be optimized in the same way as that for the previously demonstrated case. For an optimized bus without significant reflection and propagation losses inside the substrate, the intensity of the output channel with an input intensity P_{in} can be written as

$$P_{out} = \eta(1-R)P_{in}, \qquad (1)$$

where R is the reflectivity of the input grating coupler and η is the output efficiency of that channel. For a performance optimized bus line, the worst output efficiency has a value of 1.5%[5]. Without any anti-reflection coating, experiments showed $R \approx 11\%$. For the detection of the optical signal, APD (avalanche photodiode) receivers are more suitable than PIN receivers for our final packaging of the bus system. This is because of their better sensitivity and higher input power dynamic range. Higher dynamic range can be obtained with APD receivers. For short wavelength (0.8-0.9 μm) detection, Silicon APD receivers are mostly used, and a dynamic range of about 40-50 dB has been obtained. In long wavelength (1.1-1.6 μm) region, Germanium and III-V alloys such as InGaAsP and GaAlAsSb give better performances, and a dynamic range of 25-40 dB has been

reported[16]. The sensitivity of the receivers, that is, the minimum optical signal power required at the optical detector input for a desired receiver performance, determines the minimum power requirement of an optoelectronic system. For a bit error rate (BER) of 10^{-9}, operating at 500 Mbit/sec, having a multiplied primary dark current of 1000 nA, the sensitivity of Silicon APDs at 0.85 μm is around -45 dBm; for Germanium and InGaAs APDs, the sensitivities at 1.3 μm are about -41 dBm and -42 dBm, respectively[16]. All of the above sensitivities would result in a minimum signal power of around 0.04 μW at the input of the detectors. On considering the reflection from the input port, Eq. 1 gives a minimum input power of 3.0 μW, which can be easily achieved using state of the art VCSEL technology[17, 18]. Take an average dynamic range of 30 dB, the input power range over which the receivers can perform properly without distortion and saturation lies between 3.0 μW-3.0 mW.

5.2 Misalignment considerations

Several factors would affect the packaging of the hybrid backplane bus system when integrated with transmitters and receivers. Among others, the most important ones which is discussed in this section: lateral misalignment, angular misalignment, wavelength instability and divergence of spot size.

Lateral misalignment means the misalignment of the device position due to the inaccuracy on the bus plane. It can be divided into absolute and relative misalignments. With current self-aligned flip-flop solder bump bonding process[19], the absolute lateral misalignment can be controlled with an accuracy of ~1 μm. Once coupled into the substrate, the signal beam travels towards the photodetector, a lateral misalignment in the photodiode results in an equivalued spatial shift of the output signal beam.

The influence of the angular misalignment on the lateral misalignment arises from the phase mismatch between the input signal beam and the grating vector when the incident angle deviates from the Bragg angle. Fig. 10 shows the phase-matching condition of a hologram for surface-normal coupling.

For Bragg diffraction, we have[20]

$$\begin{pmatrix} -\sin\gamma \\ \cos\gamma \end{pmatrix} = \begin{pmatrix} \dfrac{\sin\theta}{n} - \dfrac{K}{\beta}\sin\phi \\ \sqrt{1 - \dfrac{\sin^2\theta}{n^2}} - \dfrac{K}{\beta}\cos\phi \end{pmatrix}, \qquad (2)$$

where n is the refraction index of the hologram, $\beta = 2\pi n/\lambda$ is the propagation constant of light with wavelength λ, and the meanings of γ, θ, and K are as shown in Fig. 10. After eliminating ϕ from Eq. (2) and differentiating the resulting equation, we have

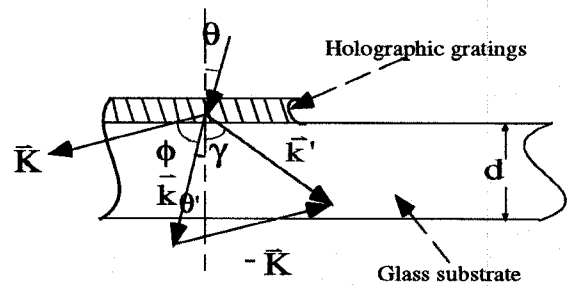

Fig 10. Phase-matching diagram correlating the grating vector $\vec{K}$, the incident beam $\vec{k}$ and the diffracted beam $\vec{k}'$ for a 1-D array of slanted holographic gratings.

$$\Delta\gamma = \frac{\left[\sin\theta - n\left(\dfrac{K^2}{2\beta^2} - 1\right)\sin\gamma\right]\cos\theta}{\left[\left(\dfrac{K^2}{2\beta^2} - 1\right)\sin\theta - n\sin\gamma\right]n\cos\gamma}\Delta\theta \qquad (3)$$

If the number of total internal reflection of the specific optical signal shown in Fig. 10 is m, then the corresponding device length is

$$L = md\tan\gamma. \qquad (4)$$

From Eqs. (3) and (4), a variation of the angle of the input optical signal will lead to a spatial shift of the fanout beam on the device surface of

$$\Delta L = \frac{\left[\tan(\gamma + \Delta\gamma) - \tan\gamma\right]}{\tan\gamma}L, \qquad (5)$$

and $\Delta\gamma$ is given by Eq. (3). This relation is schematically shown in Fig. 11 on next page. In our calculation, we have assumed the wavelength of the VCSEL as $\lambda = 850$ nm, n=1.512 (polymer waveguide), $\theta = 0°$ (surface-normal), $\gamma = 45°$, d=3.2 mm and L is taken as the longest distance, that is $(2d\tan\gamma)\times(9-1) = 5.12$ cm.

We see from Fig. 11 that within a small angular misalignment of the input optical signal, ΔL changes linearly with $\Delta\theta$, which can also be seen from Eqs. (4) and (5). However, Fig. 11 also shows that, the control of the angular alignment shouldn't be so easy a task. To keep the spatial shift of the output signal beam below an error range of ± 50 μm (for a Silicon APD, typical size of active area is in the order of ~100 μm at 1 GHz), the

angular misalignment should be within $\pm 0.03°$. This stringent requirement is significantly relaxed by applying gradient index lens (GRIN), which is to be addressed in next section.

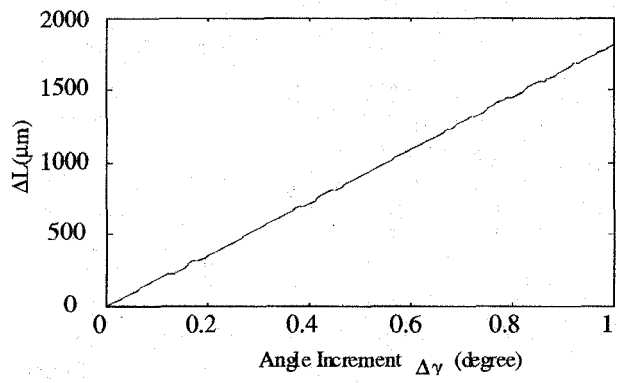

Fig. 11 Variation of spatial position of fanout beam on the device surface with respect to the angular misalignment of the input signal beam.

Variation of lasing wavelength from the transmitter influences the spatial shift of the output signal beam via the same mechanism as does the angular misalignment. In fact, this mechanism has been used in the design of a wavelength division demultiplexing (WDDM) device[21]. Theory behind this mechanism is that: a deviation in wavelength of the input signal beam will lead to an angular deviation of the diffracted beam from the Bragg angle. This comes out as the spatial shift of the output beam.

Generally, the emission line width from VCSELs can be as narrow as less than 1 $\mathring{A}$. The misalignment due to this spectral width factor can thus be determined to be 0.17 μm, which can be ignored when considering that the normal size of the photodetector active area is on the order of ~100 μm. For a VCSEL with a three-quantum-well (QW) InGaAs/GaAs active region, the lasing wavelength varies with temperature in a rate[22] of ~0.5 $\mathring{A}/°K$. To maintain a spatial shift within ± 50 μm, the allowable temperature variation is $\pm 5.8\,°K$, which is within the limit of the contemporary optoelectronic temperature stability control level[23]. An alternative method to alleviate this laser wavelength drift effect due to change in temperature is to add intermediate field holographic optical elements between neighboring boards[24].

For the VCSELs we employed, the active light emitting window has a diameter of 15 μm. Assume an TEM_{00} Gaussian emission from the VCSEL laser, after propagating a distance z in a homogenous medium, the radius of the beam spot becomes[25]

$$r(z) = r_0\left(1+\frac{z^2}{z_0^2}\right)^{1/2} \tag{6}$$

where

$$z_0 = \frac{\pi r_0^2 n}{\lambda} \tag{7}$$

and r_0 is the size of the VCSEL mirror. With z=5.12 cm in the substrate, the spot size becomes 611 μm which renders the detector impossible to respond in compare with the ~100 μm size of the detector active region for an 1 Gbit/sec system. To make the system practical, precise beam profile manipulation is required. Here we introduce GRIN (gradient index) lenses into our system as shown in Fig. 6. A 0.25 pitch GRIN lens is suitable for our application. After the signal beam from the VCSEL travels through the GRIN lens, it will get collimated. Theoretically, as long as the collimated beam keeps surface-normally incident onto the GRIN lens at the output end, it will be focused into diffraction-limited spot. Fig. 12 shows the output near field beam pattern at the end facet of the 0.25 pitch output GRIN lens that functions as a focusing element.

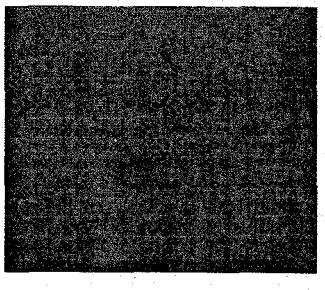

Fig. 12. Near-field profile of the focal spot shown at the output facet of the 0.25 pitch output GRIN lens with a spot size of 70 μm.

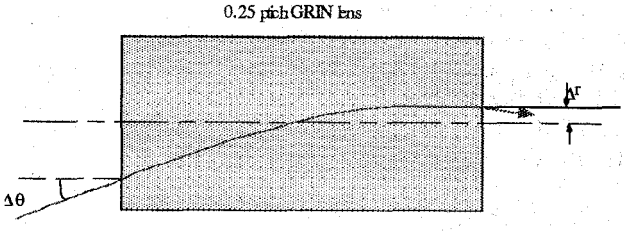

Fig. 13. Parameters in ray-tracing solution of the 0.25-pitch GRIN lens with an incident angle deviation of $\Delta\theta$.

If the input signal beam has a misalignment $\Delta\theta$ in its input angle as shown in Fig. 13, then the ray matrix[26] gives the spot shift at the focusing end as

$$\Delta r = \frac{\Delta\theta}{N_0\sqrt{A}} \qquad (8)$$

where N_0 is the refractive index on the central axis of the GRIN lens, $\sqrt{A}$ is the index gradient constant. At λ=0.85 μm, N_0=1.6457 and $\sqrt{A}$=0.423. With a misaligned angle of 2 degree, the shift of the output spot from the central axis of the GRIN lens is $\Delta r \approx 50$ μm, while without the GRIN lens, this same angular misalignment would give ~3.6 mm in reference to Fig. 11. Thus, the use of GRIN lens in our backplane bus system greatly eases the angular tolerance. The current commercially available GRIN lenses have a minimum diameter of 1 mm. For the photodetectors to collect all the output energy and to tolerate the spatial shift induced by the misalignment of the input port, the diameter of the GRIN lenses at the output port should be larger than that at the input port. The spot size shown in Fig. 12 is 70 μm (3 dB), which is less than the diameter of the photodetector employed. The enlargement is due to the Gaussian beam effect.

6. Conclusions

We have presented the hybrid optoelectonic backplane with multiple bus lines and discussed its application to a high-performance backplane bus for multiprocessor systems. Implementation and demonstration of bi-directional optical backplane buses are presented. Power budget consideration is discussed based upon previous theoretical results and a minimum input power of 3.0 μW is found to ensure the normal operation of the bus with 9 processor/memory boards for each bus line. Packaging-related issues, such as the angular misalignment and wavelength toleration are considered. Finally, a GRIN lens focusing mechanism is introduced into the hybrid system. It is found that not only can the GRIN lens function the collimating and focusing of the signal beam, but also it can greatly ease the alignment of the input channels. Future results based on a VCSEL array and a APD array will be presented in the meeting.

The authors want to thank Mr. Tchang-hun Oh for his help in the hybrid backplane structure discussion. This research is currently sponsored by DARPA's Center for Optoelectronics Science and Technology, ONR and the ATP program of the State of Texas.

References

[1]P. Sweazey, "Limits of performance of backplane buses," in *Digital Bus Handbook*, edited by J. De Giacomo, McGraw-Hill, New York, 1990.

[2]IEEE Futurebus+ P869.1: Logical Layer Specifications, Published by IEEE, New York, 1990.

[3]Ray T. Chen, "VME optical backplane bus for high performance computer," reprinted from *Optoelectronics-Device and Technologies*, 1994.

[4]J. W. Goodman, F. I. Leonberger, S.-Y. Kung, and R. A. Athale, "Optical interconnections for VLSI systems," *Proc. IEEE* **72**(7), pp. 850-866, 1984.

[5]C. Zhao, Tchang-hun Oh and Ray T. Chen, "General purpose bi-directional optical backplane: high-performance bus for multiprocessor systems," in *Proc. 2nd int'l. conference on massively parallel processing using optical interconnections*, E. Schenfeld ed., IEEE Computer Society Press, 188, 1995.

[6]J. P. G. Bristow, "Recent progress in optical backplane," presented at OE/LASE '94, Los Angeles, California 22-29 January 1994.

[7]Steven K. Case, "Coupled-wave theory of multiply exposed thick holographic gratings," *Journal of the Optical Society of America*, **vol. 65, no. 6**, p724, 1975.

[8]A. Takai, T. Kato, S. Yamashita, S. Hanatani, Y. Motegi, K. Ito, H. Abe, and H. Kodera, "200-Mb/s/ch 100-m optical subsystem interconnections using 8-channel 1.3-mm laser diode arrays and single-mode fiber arrays," *Journal of Lightwave Technology* , **vol. 12**, pp. 260-269, 1994.

[9]T. Nagahori, M. Itoh, I. Watanabe, J. Hayashi, and H. Honmou, "150 Mbit/s/ch 12-channel optical parallel interface using an LED and a PD array," *Optics and Quantum Electronics* , **vol. 24**, pp. S479-S489, 1992.

[10]R. A. Morgan, "Advances in Vertical Cavity Surface Emitting Lasers," *Proc. SPIE* , **vol. 2147**, pp. 97-119, 1994.

[11]D. Vakhshoori, J. D. Wynn, and G. J. Zydzik, "8 x 18 top emitting independently addressable surface emitting laser arrays with uniform threshold current and low threshold voltage," *Applied Physics Letters.*, **vol. 62**, pp. 1718-1720, 1993.

[12]A. von Lehmen, C. Chang-Hasnain, J. Wullert, L. Carrion, N. Stoffel, L. Florez, and J. Harbison, "Independently addressable InGaAs/GaAs Vertical cavity surface emitting laser arrays," *Electronics Letters* , **vol. 27**, pp. 583-585, 1991.

[13]R. A. Novotny, "Parallel optical data links using VCSELs," *Proc. SPIE* , **vol. 2147**, pp. 140-149, 1994.

[14]S. Tang, R. T. Chen, D. Gerald, M. M. Li, C. Zhao, S. Natarajan, and J. Lin, "Design limitations of highly parallel free-space optical interconnects based on arrays of vertical-cavity surface emitting laser diodes, microlenses, and photodetectors," *Proc. SPIE* , **vol. 2153**, pp. 323-33, 1994.

[15]Y. S. Liu, R. J. Wojnarowski, W. A. Hennessy, J. P. Bristow, Y. Liu, A. Peczalski, J. Rowlette, A. Plotts, J. Stack, J. Yardley, L. Eldada, R. M. Osgood, R. Scarmozzino, S. H. Lee and V. Uzguz, "Polymer optical

interconnect technology (POINT)-optoelectronic packaging and interconnect for board and backplane applications," *Optoelectronic Interconnects and Packaging, Critical Reviews*, **vol. CR62**, p. 405, 1996.
[16]T. V. Muoi, "Optical design for high-speed optical-fiber systems," *J. Lightwave Tech.*, **vol. LT-2**, pp. 243-267, 1983.
[17]J. L. Jewell, J. P. Harbison, A. Scherer, Y. H. Lee and L. T. Florez, "Vertical-cavity surface-emitting lasers: design, growth characterization," *IEEE J. Quantum Electron.*, **vol. QE-27**, pp. 1332-1346, 1991.
[18]K. Uomi, S. J. B. Yoo, A. Scherer, R. Bhat, N. C. Andreadakis, C. E. Zah, M. A. Koza and T. P. Lee, "Low threshold, room temperature pulsed operation of 1.5 μm vertical-cavity surface-emitting lasers with an optimized multi-quantum well active layer," *IEEE Photon. Tech. Lett.*, **vol. 6**, pp. 317-319, 1994.
[18]M. J. Wale and C. Edge, "Self-aligned flip-chip assembly of photonic devices with electrical and optical connections," *IEEE Transactions on Components, Hybrids and Manufacturing Technology*, **vol. 13**, pp. 780-786, 1990.
[20]H. Kogelnik, "Coupled wave theory for thick hologram gratings," *The Bell System Technical Journal*, **vol. 48, no. 9**, 2909, 1969.
[21]M. M. Li and Ray T. Chen, "Two-channel surface-normal wavelength division demultiplexer using substrate guided waves in conjunction with multiplexed waveguide holograms," *Applied Physics Letter*, **vol. 66, no. 3**, p262, 1995.
[22]H. Deng, C. C. Lin, D. L. Huffaker, Q. Deng and D. G. Deppe, "Temperature dependence of the transverse lasing mode in vertical-cavity lasers," *J. Appl. Phys.*, **vol. 77**, pp. 2279-2286, 1995.
[23]C. Lin, *Optoelectronic Technology and Lightwave Communications Systems* (Van Nostrand Reinhold, New York, 1989), ch. 15.
[24]H. Kobolla, N. Lindlein, O. Falkenstörefer, S. Rosner, J. Schmidt, J. Schwider, N. Streibl and R. Völkel, in *3rd IEE Conf. on Holographic Systems, Components and Applications*, p.123, 1991.
[25]A. Yariv, *Optical Electronics*, 3rd ed., Holt, CBS College Publishing, New York, p29, 1985
[26]SELFOC Product Guide, NSG American, Inc., somerset, NJ.